Responses of foraminiferal isotopic variations at ODP Site 1143 in the southern South China Sea to orbital forcing

TIAN Jun, WANG Pinxian & CHENG Xinrong

Laboratory of Marine Geology, Tongji University, Shanghai 200092, China
Correspondence should be addressed to Tian Jun (email: ian.tianjun@263.net)

Received April 14, 2003

Abstract The foraminiferal $\delta^{18}O$ and $\delta^{13}C$ records for the past 5 Ma at ODP Site 1143 reveal the linear responses of the Plio-Pleistocene climatic changes in the southern South China Sea to orbital forcing at the obliquity and precession bands. The phase of the $\delta^{18}O$ variations with the orbital forcing is opposite to that of the $\delta^{13}C$, which may be caused by the frequent El Niño events from the equatorial Pacific. The amplification of the Northern Hemisphere Ice Sheet at ~3.3 Ma probably affected the development of the 100-ka climatic cycles. Its further spreading may spur the 100-ka climatic cycle to become the dominant cycle in the late Pleistocene. The "Mid-Pleistocene Transition" event has localized influence on the isotopic variations in the southern South China Sea. The foraminiferal $\delta^{13}C$ records for the past 5 Ma at Site 1143 are highly coherent with the orbital forcing at the long eccentricity band, and lead the $\delta^{18}O$ records at the shorter eccentricity band, highlighting the importance of the carbon cycle in the global climate change.

Keywords: southern South China Sea, ODP, oxygen and carbon isotope, orbital forcing.

DOI: 10.1360/03yd0129

1 Astronomical theory

One of the greatest achievements of the Earth Sciences in the 20th century is the establishment of the Milankovitch theory or the astronomical theory[1]. As Imbrie pointed out[2], the astronomical theory can be described as a simple system model. The input to the system can be defined as changes in the geometry of the Earth's orbit or the seasonal and latitudinal distribution of incoming solar radiation, whereas the output to the system can be defined as one or more calculated climatic indices, such as the total volume of ice on land and the sea surface temperature. The entire climate system between the input and the output, with all of its complex internal mechanisms, is represented by a set of differential equations which describe how a given input to the system is transformed into specific output. For several decades, most of attempts to test this theory have been carried out in the time domain by comparing the geological record of climate with predicted climate curves. For severe demands on the adequacy of the system model, these attempts ran into serious difficulties, particularly the inaccuracy of the geological time scale and the ambiguity of climatic predictions[2]. An alternate approach, which demands fewer on the system model, is to compare the geological record with the model's input in the frequency domain[3,4]. If the system model is linear, the spectral characteristics of the output must match those of the input. The input of the simple model, such as the geometry of the Earth's orbit, has dominant periods of

413 ka or 404 ka (long eccentricity), 100 ka (eccentricity), 41 ka (obliquity), 23 ka (precession) and 19 ka (precession). However, in the observed records of deep-sea sediment properties, the periods are not identical to the input periods, but vary within a small range (table 1). For example, the model input 100 ka and 413 ka periods often behave as periods from 90 ka to 110 ka and from 350 ka to 500 ka, respectively[2]. This theory has widely been accepted for its ability to account for two climatic cycles of 41 ka and 23 ka that are phase locked to obliquity and precession respectively.

Table 1 Length of some important Pleistocene climate cycles in thousands of years[2]

Predicted by orbital theory			Observed in deep-sea cores
Driving term	Linear response models	Simple nonlinear response models	
Eccentricity	—	413 ka	350—500 ka
Eccentricity	—	100 ka	90—110 ka
Obliquity	41 ka	41 ka	40—42 ka
Precession	23 ka	23 ka	22—24 ka
Precession	19 ka	19 ka	18.5—19.5 ka

However, the interpretation of the 100-ka rhythm remains controversial if taking the climate response to orbital forcing as linear. The second controversy over the astronomical theory is the absence of the late-Pleistocene ice volume cycles in marine δ^{18}O records to match the 404-ka cycle in the earth's eccentricity. The third controversy over the astronomical theory is the interpretation of the so-called "Mid-Pleistocene Revolution" or the "Mid-Pleistocene Transition" event[5,6].

Two useful measurements to record marine sediment properties that could be linearly related to some index of climate are foraminiferal δ^{18}O and δ^{13}C, in marine microfossils the former is approximately inversely proportional to the ice volume on land and the latter is proportional to the ocean carbon reservoir[7]. In this study we will utilize the benthic and planktonic foraminiferal δ^{18}O and δ^{13}C records from ODP Site 1143 to discuss the response of the local climate change in the southern South China Sea (SCS) to orbital forcing, discussing some existing problems of the astronomical theory and attempting to give our answers.

2 Samples and methods

A total of 1992 samples of both benthic and planktonic foraminifers from upper 190.77 m at Site 1143 were measured for stable oxygen and carbon isotopes. The preparation of samples and stable isotope analyses were performed in the Laboratory of Marine Geology of Tongji University, Shanghai. The process and methods can be picked up in the reference[8]. The average time resolution of the samples is 2—3 ka. By taking the benthic foraminifer δ^{18}O as the tuning material and the obliquity and precession as the tuning target[9], a 5-Ma astronomical timescale for Site 1143 was established using an automatic orbital tuning method[10]. After the astronomical tuning, the depth of 190.77 m from Site 1143 corresponds to an age of ~5 Ma.

Spectral, cross spectral and digital filtering analyses were performed on the δ^{18}O and δ^{13}C records at Site 1143 for the past 5 Ma. One technique of the time series analysis is the spectral analysis, which is frequently used to extract rhythmic cycles embedded within the climate records. Cross spectral analysis is also an efficient way to measure the correlation between two time series at the frequency domain. We use "ARAND" program from Brown University to do the spectral and cross spectral analyses. Digital filtering is used to extract the form of individual cycles at a specific period (or narrow range of periods) from the complexity of the total signal. Usually, the band-pass filtering (filtering of a narrow band or range of the many periods actually present in a given signal) is used in the climate records. We use "ANALYSERIES" program from France to do the filtering analyses.

3 Results

3.1 Digital filtering of the isotopic records

The 100-ka components of the benthic δ^{18}O are nearly negligible prior to 3.5 Ma, whereas in the interval of 2.0—3.5 Ma, the 100-ka components increase in the amplitude and remain relatively constant in a moderate amplitude (fig. 1(b)). From 2.0 Ma to

1.5 Ma, the 100-ka components of the benthic δ^{18}O decrease in the amplitude and remain constant in a lower level. Just after 1.5 Ma, the 100-ka components of the benthic δ^{18}O gradually increase in the amplitude till to the present. The 100-ka components of the benthic δ^{18}O dominate the last 0.6 Ma, with the largest amplitude in the Plio-Pleistocene. Its average amplitude during this interval is approximate 0.15‰, nearly two times the average amplitude of 41-ka or 23-ka components, indicating the dominant role of the 100 ka cycle in the past 0.6 Ma. For the planktonic δ^{18}O (fig. 1(f)), it is just after 0.6 Ma that the 100-ka components gradually increase in the amplitude till to the present and become the dominant cycle in the Late Pleistocene. Before 0.6 Ma, the 100-ka components of the planktonic δ^{18}O are very small in the amplitude, similar to the benthic δ^{18}O record prior to 3.5 Ma. The 41-ka components of the benthic δ^{18}O remain relatively stable in the amplitude throughout the last 5 Ma, although there is a small increase in the amplitude after 2.5 Ma relative to those before 2.5 Ma (fig. 1(c)). The amplitude of the 41-ka components of the planktonic δ^{18}O is smaller than those of the benthic, and also remain relatively stable for the past 5 Ma (fig. 1(g)). The 21-ka components of the benthic δ^{18}O remain relatively stable in each of the two time intervals, 0—2.5 Ma and 2.5—5.0 Ma (fig. 1(d)). Clearly from fig. 1(d), the average amplitude of the 21-ka components of the benthic δ^{18}O is larger in the interval 0—2.5 Ma than in the interval 2.5—5.0 Ma. For the planktonic δ^{18}O records, the 21-ka components have no difference in the average amplitude between the two time intervals (fig. 1(h)). The filtering on the δ^{18}O records indicates that the 21-ka components are stronger in the planktonic δ^{18}O but weaker in the benthic δ^{18}O, whereas the 100-ka and 41-ka components are stronger in the benthic δ^{18}O but weaker in the planktonic δ^{18}O.

Like the δ^{18}O records, the 100-ka components of the benthic δ^{13}C increase in the amplitude after 0.6 Ma, and become the dominant cycle in the last 0.6 Ma

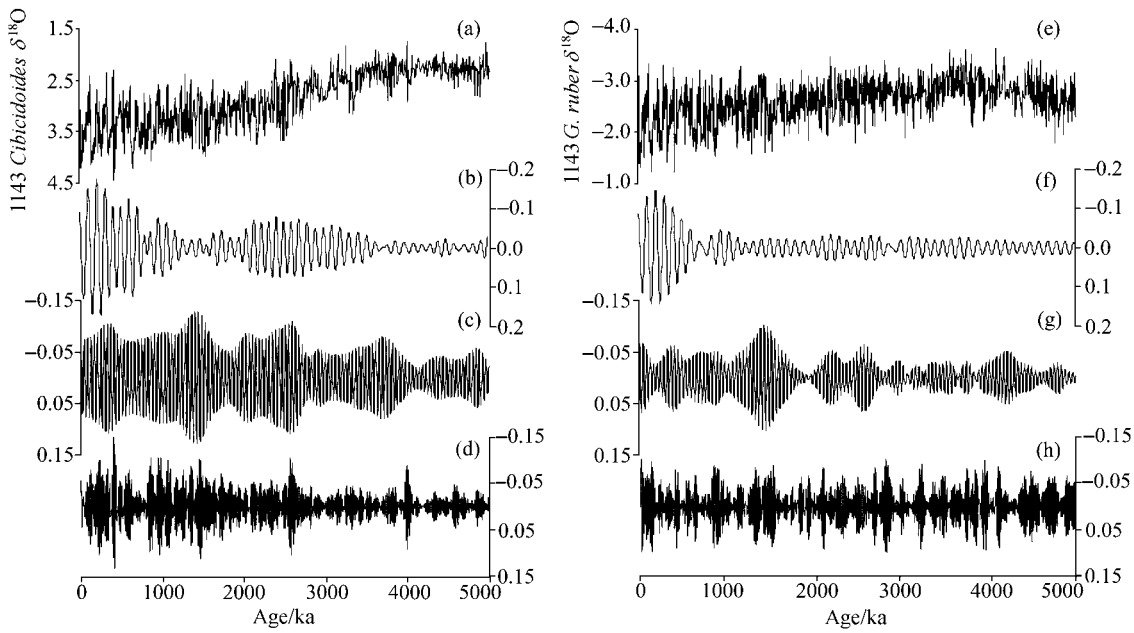

Fig. 1. Foraminiferal δ^{18}O records and their filterings at Site 1143. (a) Benthic *Cibicidoides* δ^{18}O (‰, PDB), (b), (c) and (d) are Gaussian band-pass filterings of (a) at 100 ka, 41 ka and 21 ka respectively; (e), planktonic *G. ruber* δ^{18}O (‰, PDB), (f), (g) and (h) are Gaussian band-pass filterings of (e) at 100 ka, 41 ka and 21 ka respectively. Central frequency and bandwidth are 0.01 ka^{-1} and 0.001305 ka^{-1}, 0.02439 ka^{-1} and 0.002654 ka^{-1}, 0.04761 ka^{-1} and 0.01025 ka^{-1} for 100 ka, 41 ka and 21 ka respectively.

(fig. 2(b)). Immediately prior to 1.8 Ma, the 41-ka components of the benthic δ^{13}C begin to increase in the amplitude and become the dominant cycle in the interval of 0.6—1.8 Ma (fig. 2(c)). The 21-ka components of the benthic δ^{13}C are relatively stable in the amplitude in the past 5 Ma (fig. 2(d)). The 100-ka components of the planktonic δ^{13}C is very weak in the past 5 Ma, although in some intervals the amplitude is larger (fig. 2(f)). Just after 1.5 Ma, the 41-ka components of the planktonic δ^{13}C gradually decrease till to the present, reaching a value close to zero (fig. 2(g)). This is in contrast to the benthic δ^{13}C, of which the 41-ka components remain relatively stable in the amplitude in the late Pleistocene. The 21-ka components of the planktonic δ^{13}C gradually increase in the amplitude in the last 400 ka, whereas those of the benthic δ^{13}C gradually decrease in the amplitude, reaching a value close to zero at the present (fig. 2(h) and (d)).

3.2 Cross spectrum of the isotopic records with the orbital forcing

The responses of the climate proxies to the orbital forcing may vary with time and space. Even on the same location, different climate proxies may respond differently. Are the responses of different time series coherent with orbital forcing or with one another? Are these responses synchronous within a given orbital cycle? Cross spectral analysis has the ability to measure the coherency and phase between two time series, and therefore could answer the above questions in part.

(ⅰ) Coherency. Cross spectrums between the isotopic records of Site 1143 and the ETP are analyzed at intervals of 0—5 Ma. ETP is the sum of the normalized eccentricity, normalized obliquity and normalized negative precession. Table 2 shows the values of coherency and phase, whereas fig. 3. illustrates the spectrum and coherency. It is clear from fig.3 that all of the isotopic spectrums contain moderate to strong 41-ka and 23-ka peaks, and all the records are coherent with the ETP at both obliquity and precession bands. Generally, for an individual isotopic record, the coherency at the obliquity band is the highest among the three coherencies at the eccentricity, obliquity and precession bands, such as that of the benthic $-\delta^{18}$O. Although all time series contain moderate to strong 100-ka cycles, only the benthic $-\delta^{18}$O and δ^{13}C are coherent with the ETP at the eccentricity band (fig. 3(a) and (c)). The planktonic $-\delta^{18}$O and δ^{13}C records are not coherent with the ETP at the eccentricity band (fig. 3(b) and (d)). The benthic δ^{13}C contains strong 41-ka

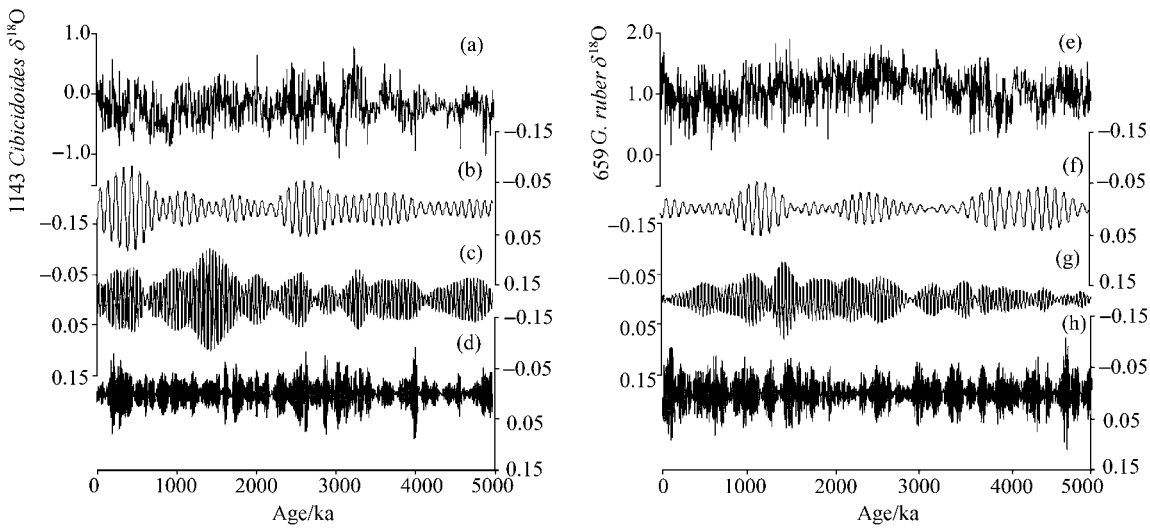

Fig. 2. Foraminiferal δ^{13}C records and their filterings at Site 1143. (a) benthic *Cibicidoides* δ^{13}C (‰, PDB), (b), (c) and (d) are Gaussian bandpass filterings of (a) at 100 ka, 41 ka and 21 ka respectively; (e), planktonic *G. ruber* δ^{13}C (‰, PDB), (f), (g) and (h) are Gaussian bandpass filterings of (e) at 100 ka, 41 ka and 21 ka respectively. Filtering parameters refer to fig. 1.

Table 2 Phase relationships and coherency between ETP (sum of normalized eccentricity, normalized obliquity and normalized negative precession) and isotopic records of Site 1143 for the past 5 Ma

	100 ka (eccentricity)		41 ka (obliquity)		23 ka (precession)		19 ka (precession)	
	coherency	phase/(°)	coherency	phase/(°)	coherency	phase/(°)	coherency	phase/(°)
$-\delta^{18}$O(b)	0.7761	134 ± 22	0.9866	113 ± 7.9	0.8692	87 ± 15.7	0.8778	88.5 ± 15
$-\delta^{18}$O(p)	—	—	0.8973	121 ± 17.9	0.9367	108 ± 32	0.8587	17.5 ± 16
δ^{13}C (b)	0.7412	−60 ± 24.2	0.9231	93.5 ± 11.7	0.8202	98.5 ± 19.1	0.7211	134 ± 25
δ^{13}C (p)	—	−62.8 ± 29	0.9043	117 ± 13.2	0.8546	119 ± 16.8	0.7614	162 ± 23

Test statistics at 80% level for non-zero coherency = 0.707267. Coherency lower than this value is represented by dashed lines. “b” denotes benthic foraminifers. “p” denotes planktonic foraminifers.

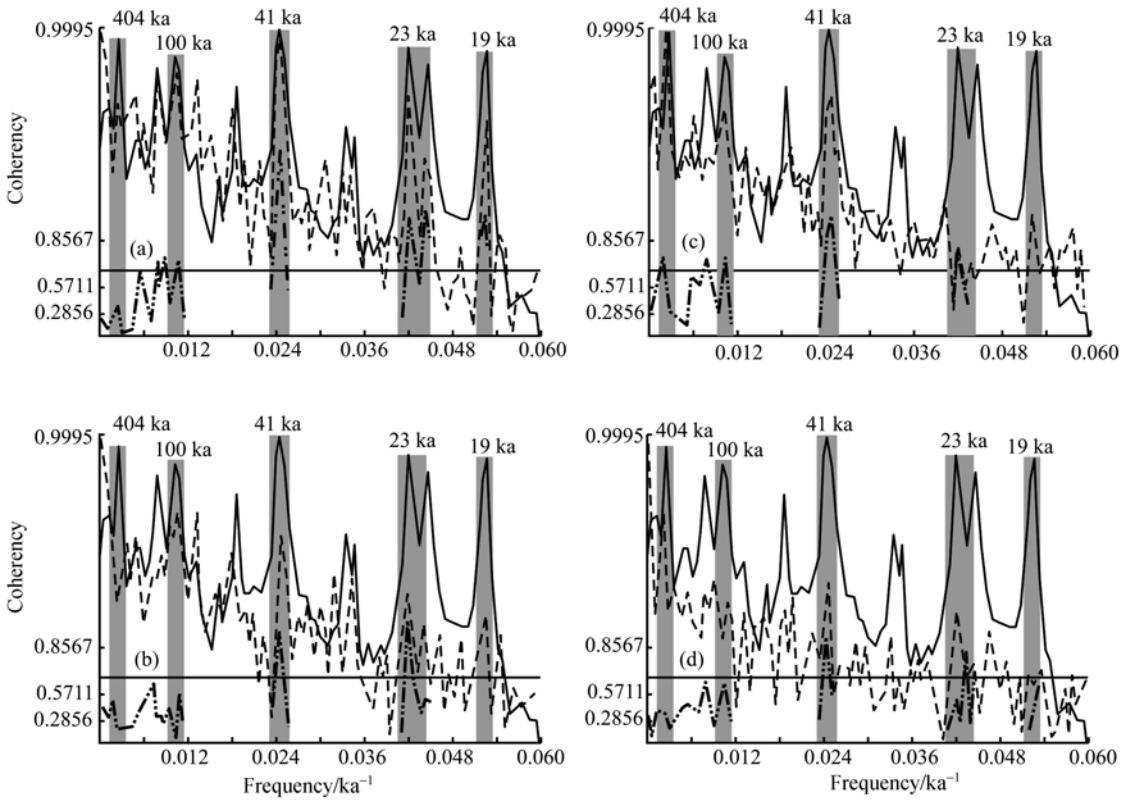

Fig. 3. Cross spectrums of ETP with (a) *Cibicidoides* $-\delta^{18}$O, (b) *G. ruber* $-\delta^{18}$O, (c) *Cibicidoides* δ^{13}C and (d) *G ruber* δ^{13}C from ODP Site 1143 for the past 5 Ma. Spectral densities are normalized and plotted on a log scale. Solid lines denote the spectrum of ETP. Dashed lines denote the spectrum of isotopes. Dotted dashed line denote the coherency. The coherency spectra are plotted on a hyperbolic arctangent scale. The non-zero coherencies at 80% level are represented respectively by the horizontal solid lines. Grey areas denote the range of the orbital periods of 404 ka, 100 ka, 41 ka, 23 ka and 19 ka.

signals but weak 23-ka signals, whereas planktonic δ^{13}C contains weak 41-ka signals but strong 23-ka signals (fig. 3(c) and (d)). Both the benthic and planktonic δ^{13}C records contain strong periods near 404 ka, and the benthic δ^{13}C is coherent with the ETP at the 404-ka band. The 404-ka power density of benthic δ^{13}C is as high as that of ETP and the non-zero coherency is above 80%. Though there is also a weaker 404-ka cycle in the spectrum of benthic $-\delta^{18}$O relative to that of the ETP, the coherency between them is lower than 80% statistical level and therefore indicates no coherent relationships between them. In general, the responses of both benthic and planktonic isotopic records from Site 1143 in the past 5 Ma are linearly

coherent with the orbital forcing (ETP) at the obliquity and precession bands, and only the benthic δ^{13}C records are linearly coherent with the orbital forcing at the eccentricity band.

(ⅱ) Phase. As shown in table 2 and fig. 4, all of the four isotopic series (benthic and planktonic $-\delta^{18}$O and δ^{13}C maxima) lag the ETP (Northern Hemisphere summer insolation maxima) at the obliquity band. The phase of each isotopic series with the ETP varies from 93.5° to 117° (fig. 4(b)), with an average of 111°. In view of the phase errors which change from 7.9° to 13.2°, the phase of each isotopic series with the ETP can be taken as equal at the obliquity band. The phase relationship at the 23-ka precession band is identical to that at the obliquity band. All the four isotopic series show a lag phase with the ETP, which vary from 87° to 119° (fig. 4(c)). Considering the phase errors varying from 16.8° to 32°, the phase for each of the isotopic series at the 23-ka precession band can still be regarded as equal. The phases described above indicate synchronous responses of the four climatic indices to the external at the 41-ka obliquity and the 23-ka precession bands in the past 5 Ma. However, at the 19-ka precession band, the phases of four isotopic series separate away from one another too much to be taken as equal (fig. 4(d)). Therefore, the responses of the four isotopic series are not synchronous at this precession band. At the 100-ka eccentricity band, the phase of the oxygen isotopic series is nearly opposite to the phase of the carbon isotopic series (fig. 4(a)), indicating contrasting responses to the orbital forcing.

Table 3 and fig. 5 further clarify the phase relationships between the benthic $-\delta^{18}$O and δ^{13}C at the three major Milankovitch cycles in two time intervals. In the time interval 0—2.5 Ma, the benthic $-\delta^{18}$O (minimum global ice volume) leads the benthic δ^{13}C (maximum continental biomass) at the three major Milankovitch cycles, whereas at time intervals of 2.5—5.0 Ma, the benthic $-\delta^{18}$O leads the benthic δ^{13}C only at the 41-ka obliquity band and the 23-ka precession band, but lags the benthic δ^{13}C at the eccentricity band by about 20°±15°. At Site 1143, the phase relationship at the 41-ka and 23-ka bands between the benthic δ^{13}C and the benthic $-\delta^{18}$O agrees in most features with those of Sites 849 and 846[11,12]. The difference is that at Site 1143 of the West Pacific, at time intervals of 0—2.5 Ma, the benthic δ^{13}C lags the benthic $-\delta^{18}$O by about 4°±13° at the eccentricity band, whereas at Site 849 of the East Pacific, the ben-

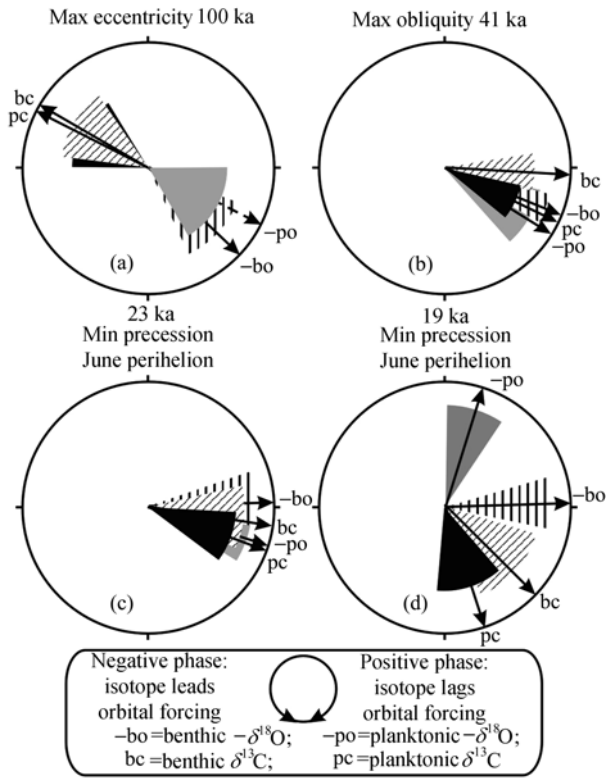

Fig. 4. Phase wheels at Site 1143 of benthic $-\delta^{18}$O, benthic δ^{13}C, planktonic $-\delta^{18}$O and planktonic δ^{13}C with the ETP, at (a) 100-ka band; (b) 41-ka band; (c) 23-ka band and (d) 19-ka band. The phase is the average in the last 5 Ma.

Table 3 Phase relationship and coherency between benthic $-\delta^{18}$O and δ^{13}C at Site 1143 in the past 5 Ma

Time interval	100 ka (eccentricity)		41 ka (obliquity)		23 ka (precession)	
	coherency	phase/(°)	coherency	phase/(°)	coherency	phase/(°)
0 2.5 Ma	0.8738	–19.7 ± 15	0.9776	26.2 ± 6.1	0.7763	41.9 ± 21.9
2.5 5 Ma	0.9022	4.0 ± 13.3	0.9392	43.2 ± 10.3	0.6851	29.8 ± 27.8

Test statistics for non-zero coherency at 80% level = 0.707267.

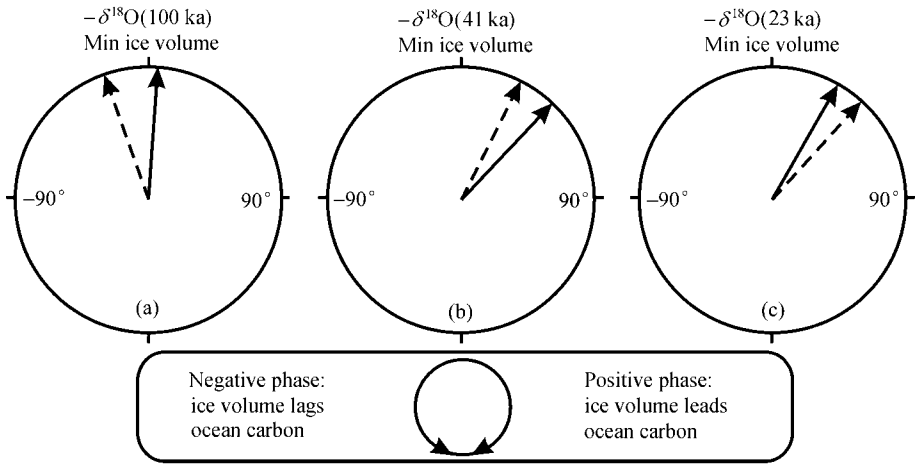

Fig. 5. Phase wheels at Site 1143 of the benthic δ^{13}C and the benthic $-\delta^{18}$O at (a) 100-ka band; (b) 41-kar band and (c) 23-ka band. Solid line with arrow denotes the phase at intervals of 2.5—5.0 Ma. Dashed line with arrow denotes the phase at intervals of 0—2.5 Ma.

thic δ^{13}C leads the benthic $-\delta^{18}$O by 12°±12° at the same time interval.

4 Discussion

4.1 Synchronous or asynchronous responses

As demonstrated by cross spectral analyses of the four isotopic series with the ETP, the Plio-Pleistocene climate in the southern SCS responds linearly to the orbital forcing at the obliquity and precession bands. The four isotopic responses at the 41-ka obliquity and 23-ka precession bands are synchronous in the southern SCS, whereas at the 19-ka precession band, the responses are asynchronous. Even more strange is that the responses of the $-\delta^{18}$O and δ^{13}C are opposite at the 100-ka eccentricity band. All of the above conclusions are based on the analysis of a stationary δ^{18}O phase with the orbits, which is just the theoretical premise of the astronomically tuned timescale of Site 1143[8]. No direct evidence exists for a nonstationary phase relationship between Plio-Pleistocene ice volume and orbital parameters[13]. Taking the benthic $-\delta^{18}$O as the standard, the isotopic series which lead the benthic $-\delta^{18}$O can be referred to as early response group, and those in phase with or slightly lagging the benthic $-\delta^{18}$O can be referred to as late response group [14]. The early spatial responses occur in deep waters of the South Atlantic and Antarctic oceans, and in surface waters of the Antarctic and tropical oceans; whereas the late spatial responses occur on land, at a range of depths in the open boreal ocean, and in low-latitude intermediate waters[14]. The planktonic δ^{18}O and δ^{13}C at Site 1143 are from the surface waters of the tropical oceans, therefore they should behave as early responses according to the standard of Imbrie et al.[14]. But at both the obliquity and precessions, they slightly lag the benthic $-\delta^{18}$O (fig. 4(b) and (c)), behaving as late responses, contradicting with the former partition. The benthic δ^{13}C at Site 1143 is from the low-latitude intermediate waters, and should behave as late response according to the standard of Imbrie et al. (1992)[14] Whereas at the obliquity band, it leads the benthic $-\delta^{18}$O and behave as the early response (fig. 4(b)), also contradicting with its previous partition. What force shifts the phase relationships of the climatic indices with the global ice volume change as represented by the benthic δ^{18}O? As Clement et al. (1999) pointed out[15], changes in the ENSO behavior can result in a mean tropical climate change, and such a change in the tropical climate can generate a globally synchronous climate response to orbital forcing. Therefore the anomalous phase relationship of the isotopic variables relative to the benthic $-\delta^{18}$O in the

southern SCS can be attributed to the ENSO events which have been frequently occurring along the equatorial Pacific.

4.2 Mid-Pleistocene transition

Since Prell (1982) found the transition of the dominant cycles from 41-ka to 100-ka before and after 0.9 Ma in the δ^{18}O records from DSDP Site 502B[16], this transition has been found in many climatic variables world-wide[5,6,17,18]. The digital filtering of both benthic and planktonic δ^{18}O at the 100-ka and 41-ka bands further demonstrate the existence of this transition in the southern SCS. Clearly from Fig. 1(b) and (f)), the amplitude of the 41-ka δ^{18}O components is larger than that of the 100-ka δ^{18}O components in the early Pleistocene and the Pliocene. From 1.5 Ma to 0.7 Ma, though the 100-ka components of the benthic δ^{18}O gradually increase in the amplitude, they are still smaller than the amplitude of the 41-ka components. Just after 0.7 Ma, the amplitude of the 100-ka components exceeds those of the 41-ka components, indicating the transition of the dominant cycle from 41-ka to 100-ka in the variations of the deep water properties in the southern SCS. This transition occurs later in the planktonic δ^{18}O, at about 0.5 Ma. However, this transition is not obviously recorded in the δ^{13}C (fig. 2(b) and (f)). Because the increase of the 100-ka δ^{18}O components in amplitude is gradual, the transition of the dominant climatic cycles can then be interpreted as a stepwise but not an abrupt process. The absence of this event in the foraminiferal δ^{13}C records from Site 1143 suggests the limited influence of the transition. This transition is not obvious in all the climatic variables even from a single place.

Although the so-called “Mid-Pleistocene Transition” is clear in many climatic variables, it still remains as an enigma why the 41-ka to 100-ka climatic transition occurred in the mid-Pleistocene but not earlier or later. As the contribution of the Earth’s eccentricity with a 100-ka periodicity to the total solar radiation change is less than 0.1%[3,19], a satisfactory answer cannot be obtained from the changes of the orbital parameters themselves. The shift may have arisen from ice sheet dynamics of high latitude when the ice volume in the Northern Hemisphere exceeded a certain threshold value[20]; or the shift was probably a response to the global carbon cycle that generated changes in atmospheric CO_2 concentration[21]. Evidence from numerical models suggests that cycles of about 10 ka in length may be required to explain the high amplitude of the 100-ka cycles[22], therefore Rutherford and Hondt (2000)[23] concluded that the increased heat flow across the equator or from the tropics to higher latitudes around 1.5 Ma ago strengthened the semi-precession cycle in the Northern Hemisphere, and triggered the transition from 41-ka cycles to sustained 100-ka glacial cycles. On the whole, there are two different viewpoints concerning the mechanism of the “Mid-Pleistocene Transition”, the high-latitude ice sheet forcing and the tropical forcing. Still, a great number of studies need to be done before this problem can be clarified.

4.3 The 100-ka and 404-ka cycles

The explanation of the observed 100-ka climate cycle in terms of astronomical theory remains controversy. One of the debating sources arises from the fact that eccentricity affects insolation mainly by modulating the precession and its direct contribution to the total radiation is too small to affect the climate change directly[3,19]. When did the 100-ka climatic cycle strengthen? Recent study thinks that this may happen around 1.5 Ma ago[23]. However, fig. 1(b) clearly shows that the 100-ka cycle of the benthic δ^{18}O from Site 1143 already strengthened in the amplitude at intervals of 2.0—3.3 Ma. The amplitude in this time interval has reached the level in the early Late Pleistocene. The same results can be shown in the 100-ka band-pass filtering of the δ^{18}O records from the east equatorial Pacific and the Atlantic[11,24]. Combining the filtering results, we may suggest that the amplification of the Northern Hemisphere ice sheet around 3.3 Ma ago probably affects the development of the 100-ka climate cycle, and the further amplification of the Northern Hemisphere ice sheet may make the 100-ka cycle the dominant climate cycle in the Late Pleistocene.

Another problem of the astronomical theory is the absence of the late-Pleistocene ice volume cycles in marine δ^{18}O records to match the 404-ka cycle in the Earth's eccentricity. As seen from fig. 3(a), an unnoticeable peak of 404-ka cycle occurs in the spectrum of the benthic δ^{18}O from Site 1143, which just matches with the 404-ka cycle in the ETP. Unfortunately, the coherency at this period with the ETP is too low to regard the 404-ka benthic δ^{18}O cycle as a linear response.

However, if we measure the coherency of the benthic δ^{18}O with the truncated insolation at 65°N (value>0) in the time interval 1.2—5.0 Ma, we will find a strong correlation between them, not only at the 404-ka cycle, but also at the 124- and 95-ka cycles, closely matching the three main eccentricity in terms of periods (fig. 6). High coherencies of the δ^{18}O with the truncated insolation at the eccentricity bands suggest that the δ^{18}O response prefers warmer portions of the insolation cycle to colder portions. The energy balance model of Short et al. (1991)[22] indicates that the spectral variances of the modeled sea surface temperature are transferred from the precession band to the 404- and 100-ka eccentricity bands within the maximum temperature response of the tropics. This transfer is due to the interaction of perihelion with the overhead passage of the Sun at either equinox, which serves to truncate the effects of the lower portions of the tropical insolation cycle resulting in concentrations of power in the temperature spectrum at 404- and 100-ka periods[22]. The ice-albedo feedback may be involved in truncating the effects of high-latitude insolation forcing, providing a high-latitude means of transferring variance via truncation[25]. The low-frequency ice volume cycles originate through an asymmetrical response mechanism that preferentially introduces variances into the climate system from the warm portions of the eccentricity-modulated precession cycle[25]. The results from this study may suggest that the climate responses to the warm and cold parts of the insolation may be asynchronous before the Late Pleistocene. This interpretation invokes a simple nonlinear response to insolation forcing, which seems to be appropriate to explain the pre-ice-age climate spectrum.

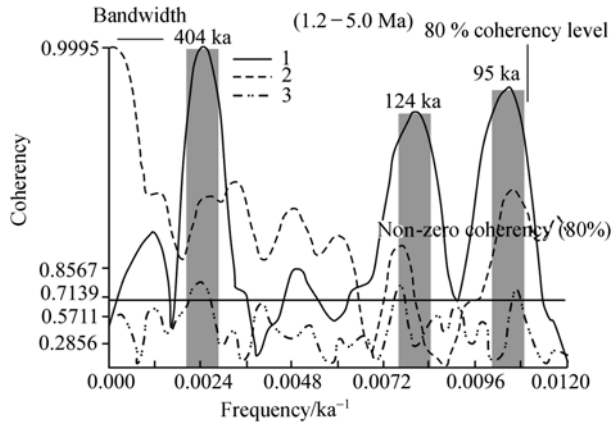

Fig. 6. Cross spectral comparison of Site 1143 benthic $-\delta^{18}$O and truncated insolation (July 65°N) for the interval of 1.2—5.0 Ma. Spectral densities are normalized and plotted on log scales. The coherence spectrum is plotted on a hyperbolic arctangent scale. Horizontal solid line denotes the 80% non-zero coherency. 1 and 2, Spectra of insolation and $-\delta^{18}$O; 3, the coherency.

Cross-spectrums of the benthic δ^{13}C from Site 1143 and the ETP reveals high coherency at the 404- and 100-ka eccentricity bands for the past 5 Ma (fig. 3(c)). The middle point of the ETP spectrum at this band points to ~404 ka, whereas that of the δ^{13}C points to ~460 ka, as well as the middle point of the coherency spectrum. Why does the 404 ka period in the ETP change to 460 ka in the δ^{13}C? It remains a question waiting for further work to answer. The negative phase of the δ^{13}C with the ETP at the 100-ka band (table 2) indicates the maximum of the eccentricity lagging the maximum of the δ^{13}C, an impossible forcing mechanism. Although a prominent ~460-ka cycle also occurs in the spectrum of the planktonic δ^{13}C (fig. 3(d)), its coherency with the ETP is much lower than the test statistics, so is the coherency with the truncated insolation at 65°N. It seems that the climate truncating response to insolation forcing only applies to the δ^{18}O, but not to the δ^{13}C, which is related to the global carbon cycle being rather unique among the climate variables. By using the record of δ^{18}O in atmospheric oxygen trapped in Antarctic ice at Vostok[26], Shackleton (2000) separated the δ^{18}O signals of ice volume, deep-water temperature, and additional processes affecting air δ^{18}O (that is, a

varying Dole effect)[21]. Based on the mathematical analysis, Shackleton (2000) found[21] that at the 100-ka period, atmospheric carbon dioxide, Vostok air temperature, and deep-water temperature are in phase with orbital eccentricity, whereas ice volume lags these three variables. Combined with the phase relationship of δ^{18}O and δ^{13}C at Site 1143, we suggest that the 100-ka cycle did not arise directly from ice sheet dynamics; instead, it was probably the response of the global carbon cycle that generates the eccentricity signal by causing changes in atmospheric carbon dioxide concentration. This inference highlights the role of the global carbon cycle in the global climate change, and therefore highlights the complexity and importance of the marine δ^{13}C records.

5 Conclusions

The foraminiferal stable δ^{18}O and δ^{13}C records from Site 1143 for the past 5 Ma suggest that the Plio-Pleistocene climate in the southern SCS responds linearly to the orbital forcing at the obliquity and precession bands. The climate responses recorded by the isotopic records are synchronous in the southern SCS at the 41-ka obliquity and 23-ka precession bands, whereas at the 19-ka precession band the responses are asynchronous. The phase of the foraminiferal $-\delta^{18}$O variations with the orbital forcing is opposite to that of the δ^{13}C variations, which may be caused by the frequent El Niño events from the equatorial Pacific. The digital filtering reveals the existence of the "Mid-Pleistocene Transition" event in the foraminiferal δ^{18}O records in the southern SCS, however, this transition happened later by ~0.2 Ma in the planktonic δ^{18}O than in the benthic δ^{18}O. The absence of this transition event in the δ^{13}C records from Site 1143 may suggest the limited influence of this event. The amplification of the Northern Hemisphere ice sheet around 3.3 Ma ago probably affect the development of the 100-ka climate cycle, and the further amplification of the northern hemisphere ice sheet may make the 100-ka cycle the dominant climate cycle in the Late Pleistocene. At the periods from 404 ka to 460 ka, the foraminiferal δ^{13}C records are highly coherent with orbital forcing. At the 100-ka period, variations of foraminiferal δ^{13}C leads that of $-\delta^{18}$O, which may indicate that the 100-ka cycle did not arise directly from ice sheet dynamics, and instead, it was probably the response of the global carbon cycle that generates the eccentricity signal by causing changes in atmospheric carbon dioxide concentration.

Acknowledgements This work was supported by the National Natural Science Foundation of China (Grant No. 4999560) and the National Key Basic Research Special Foundation (Grant No. G2000078500). The used samples were provided by the Ocean Drilling Program (ODP). ODP is sponsored by the U.S. National Science Foundation (NSF) and participating countries under management of Joint Oceanographic Institutions (JOI), Inc.

References

1. Milankovitch, M., Mathematische Klimalehre und astronomishe Theorie der Klimasch-wankungen (eds.W. Koppen, R. Geiger), Handbuch der Klimatologie, Gebruder Borntraeger, Berlin, 1930, Ⅰ(A): 1—76.
2. Imbrie, J., Astronomical theory of the Pleistocene ice ages: A brief historical review, ICARUS, 1982, 50: 408—422.[DOI]
3. Hays, J. D., Imbrie, J., Shackleton, N. J., Variations in the earth's orbit: pacemaker of the ice ages. Science, 1976, 194: 1121—1132.
4. Imbrie, J., Hays, J. D., Martinson, D. G. et al., The orbital theory of Pleistocene climate: Support from a revised chronology of the marine δ^{18}O record (ed. A. Berger), Milankovitch and Climate, D. Reidel, Norwell, Mass., 1984, 269—305.
5. Berger, W. H., Bickert, T., Schmidt, H. et al., Quaternary oxygen isotope records of pelagic foraminifers: Site 806, Ontong Java Plateau (eds. W. H. Berger, L. W. Mayer), Proc. ODP Sci. Results 130, 1993, 381—395.
6. Wang, P., Tian, J., Cheng, X. Transition of Quaternary glacial cyclicity in deep-sea records at Nansha, the South China Sea, Science in China, Ser. D, 2001, 44(10): 926—933. [Abstract] [PDF]
7. Shackleton, N. J., Opdyke, N. D., Oxygen isotope and paleomagnetic stratigraphy of equatorial Pacific core V28-238: Oxygen isotope temperatures and ice volumes on a 105 year and 106 scale, Quaternary Research, 1973, 3: 39—55.
8. Tian, J., Wang, P. X., Chen, X. R. et al., Astronomically tuned Plio-Pleistocene benthic δ^{18}O records from South China Sea and Atlantic-Pacific comparison. Earth and Planetary Science Letters, 2002, 203: 1015—1029. [DOI]
9. Laskar, J., The chaotic motion of the solar system: A numerical estimate of the size of the chaotic zones, Icarus, 1990, 88: 266—291. [DOI]
10. Yu, Z. W., Ding, Z., An automatic orbital tuning method for paleoclimate records, Geophysical Research Letters, 1998, 25: 4525—4528. [DOI]
11. Mix, A. C., Le, J., Shackleton, N. J., Benthic foraminiferal stable isotope stratigraphy of site 846: 0—1.8 Ma (eds. N. G. Pisias, L. A. Mayer, T. R. Janecek), Proc. ODP Sci. Results 138, 1995, 839—854.

12. Mix, A. C., Pisias, N. G., Rugh, W. et al., Benthic foraminifer stable isotope record from site 849 (0—5 Ma): local and global climate changes, Proc. ODP Sci. Results 138 (eds. N. G. Pisias, L. A. Mayer, T. R. Janecek), 1995, 371—412.
13. Clemens, S. C., Murray, D. W., Prell, W. L., Nonstationary phase of the Plio-Pleistocene Asian monsoon, Science, 1996, 274: 943—948. [DOI]
14. Imbrie, J., Boyle, E., Clemens, S. et al., On the structure and origin of major glaciation cycles, 1, Linear responses to Milankovitch forcing, Paleoceanography, 1992, 7: 701—738.
15. Clement, A., Seager, R., Cane, M., Orbital controls on the El Niño/Southern Oscillation and the tropical climate, Paleoceanography, 1999, 14: 441—456. [DOI]
16. Prell, W. L., Oxygen and carbon isotope stratigraphy for the Quaternary of Hole 502B: Evidence for two modes of isotopic variability (eds. W. L. Prell, J.V. Gardner), Init. Repts 68, 1982, 455—464.
17. Liu, T. S., Ding, Z. L., Rutter, N., Comparison of Milankovitch periods between continental loess and deep sea records over the last 2.5 Ma, Quaternary Science Reviews, 1999, 18: 1205—1212. [DOI]
18. Schmieder, F., Dobeneck, T. von, Bleil, U., The Mid-Pleistocene climate transition as documented in the deep South Atlantic Ocean: initiation, interim state and terminal event, Earth and Planetary Science Letters, 2000, 179: 539—549. [DOI]
19. Imbrie, J., Berger, A., Boyle, E. et al., On the structure and origin of major glaciation cycles, 2, The 100000-year cycle, Paleoceanography, 1993, 8: 699—735.
20. Berger, W. H., Jansen, E., Mid-Pleistocene climate shift—— The Nansen connection, Geophysical Monograph, 1994, 84: 295—311.
21. Shackleton, N. J., The 100000-year ice-age cycle identified and found to lag temperature, carbon dioxide, and orbital eccentricity, Science, 2000, 289: 1897—1902. [DOI]
22. Short, D. A., Mengel, J. G., Crowley, T. J. et al., Filtering of Milankovitch cycles by Earth's geography, Quaternary Research, 1991, 35: 157—173.
23. Rutherford, S., Hondt, S. D., Early onset and tropical forcing of 100,000-year Pleistocene glacial cycles, Nature, 2000, 408: 72—75. [DOI]
24. Tiedemann, R., Sarnthein, M., Shackleton, N. J., Astronomic timescale for the Pliocene Atlantic $\delta^{18}O$ and dust flux records from Ocean Drilling Program Site 659, Paleoceanography, 1994, 9: 619—638. [DOI]
25. Clemens, S. C., Tiedemann, R., Eccentricity forcing of Pliocene-Early Pleistocene climate revealed in a marine oxygen-isotope record, Nature, 1997, 385: 801—804. [DOI]
26. Petit, J. R., Jouzel, J., Raynaud, D. et al., Climate and atmospheric history of the past 420000 years from the Vostok ice core, Antarctica, Nature, 1999, 399: 429—436. [DOI]